Indian Journal of Pure & Applied Physics
Vol. 63, June 2025, pp. 544-559
DOI: 10.56042/ijpap.v63i6.18834

Structural Modification of Sol-Gel derived Nickel Ferrite and its derivatives via Rare Earth Doping and Its Impact on Electrical Properties

Sanchit Kumar[1], Chaitali Mondal[2], Amisha Raj Singh[3] & Ankurava Sinha[1*]

[1]P.G. Department of Physics, Magadh University, Bodh Gaya 824 234, India

[2]Department of Physics, Vivekananda Mahavidyalaya, Burdwan 713 103, India

[3]P.G. Department of Physics, Patliputra University, Patna 800 020, India

Received: 16 April 2025; accepted: 19 May 2025

Nickel ferrite ($NiFe_2O_4$), known for its exceptional magnetic behaviour and high electrical resistance, is commonly used in magnetic sensors, transformers, and high-frequency electronics. However, its inherent electrical qualities frequently require improvement for application in more demanding technological situations. This paper examines the structural and electrical evolution of nickel ferrite generated in sol-gel using rare earth (RE) ions such Gd^{3+}, La^{3+}, Nd^{3+}, Sm^{3+}, and Ho^{3+}. Because of their greater ionic sizes and different electronic structures, these dopants cause significant lattice distortions, change cation site distributions, and, at higher concentrations, generate secondary non-spinel phases. These alterations greatly impact electron transport by affecting the Fe^{2+}/Fe^{3+} hopping process. This allows for manipulation of resistivity and dielectric characteristics. The article also examines how critical synthesis parameters, such as solution pH and combustion agent selection, affect phase formation and microstructural uniformity. RE replacement improves the dielectric constant, loss characteristics, and electrical conductivity of these modified ferrites, highlighting their potential in applications such as electromagnetic interference (EMI) shielding, energy storage systems, and downsized electronic components. The research continues by discussing optimization tactics for dopant inclusion and synthesis conditions in order to modify functional features of Nickel ferrite family for future device integration.

Keywords: Nickel ferrite, Rare Earth doping, Sol-gel method, Structural modification, X-ray diffraction, Dielectric properties, Polaron hopping, Electrical conductivity

1 Introduction

Ferrites, especially nickel ferrite ($NiFe_2O_4$), are magnetic materials made from iron oxide and other metallic elements. They are extensively used in telecommunications, transformers, sensors, and magnetic recording[1–4]. Their distinct electrical and magnetic properties make them suitable for industrial and scientific applications. Nickel ferrite is particularly suitable for materials used to suppress electromagnetic interference (EMI) and devices such as inductors due to its soft magnetic properties, high electrical resistivity, and ability to withstand harsh environments[5-6].

The flexibility of ferrites depends on their capacity to change their characteristics. Researchers can affect crucial features like electrical conductivity and magnetic permeability by changing their chemical makeup or adding dopants. These changes are necessary for new technologies in high-frequency electronics and energy storage systems[7-8]. Doping ferrite with rare earth (RE) elements has been one of the most successful ways to improve its characteristics.[2]

Rare earth elements such as neodymium (Nd), gadolinium (Gd), and lanthanum (La) can be added to ferrites to drastically alter their electrical, magnetic, and structural characteristics. These elements distinct electronic configurations and greater ionic radii cause lattice distortions that alter the spinel structure's cation distribution, improving dielectric performance. Applications needing high-frequency and high-temperature capability will benefit from these changes[9-10]. Although pure nickel ferrite frequently exhibits unsuitable qualities for sophisticated uses, rare earth doping can enhance its transport and dielectric properties, making it more appropriate for energy conversion systems, magnetic storage devices, and microwave devices[11-12]. Additionally, Ni-based polymer nanocomposites such as poly(O-toluidine) doped with NiO or V_2O_5 have demonstrated enhanced electrical conductivity and dielectric performance, reinforcing the potential of Ni-containing systems in advanced electronic applications[13-14].

*Corresponding author: (E-mail: sinhaankurava24@gmail.com)

The effects of rare earth doping on the electrical and structural characteristics of nickel ferrite will be reviewed in this paper[15] with particular attention paid to modifications in the lattice structure, the development of secondary phases, and synthesis methods that maximize its performance for advanced technological uses[16].

2 Different Types of Ferrites

Ferrites represent an extensive category of ferrimagnetic ceramic substances that can be systematically categorized according to their magnetic characteristics (hard and soft ferrites) as well as their crystalline architectures (spinel, garnet, hexaferrite, and orthoferrite). Each unique classification plays a crucial role in determining their respective applications within the fields of technology, electronics, and magnetic devices. Here is a detailed explanation of the previously mentioned classifications.

2.1 Classification Based on Magnetic Properties

2.1.1 Hard Ferrites

Hard ferrites, sometimes referred to as permanent magnets, are distinguished by their high remanence, high coercivity (resistant to demagnetization), and long-term magnetic retention. For devices like motors, loudspeakers, and magnetic storage that need a steady magnetic field, these ferrites are perfect[17]. Due to its inherent crystal structure and the robust exchange contacts between iron ions in the lattice, hard ferrites have a high coercivity, which also contributes to their magnetic anisotropy. some examples are Barium hexaferrite ($BaFe_{12}O_{19}$), Strontium ferrite ($SrFe_{12}O_{19}$), Yttrium Iron Garnet ($Y_3Fe_5O_{12}$ - YIG)[18–20].

2.1.2 Soft Ferrites

Soft ferrites are perfect for applications requiring frequent reversal of magnetization, such as transformers, inductors, and electromagnetic interference (EMI) suppression, because of their low coercivity and ease of magnetization and demagnetization[21]. Soft ferrites are appropriate for high-frequency applications because of their high electrical resistivity, which lowers eddy current losses.

Soft ferrites are essential parts of high-frequency applications like power electronics and telecommunications because they can withstand high magnetizing currents without suffering appreciable energy losses. Some of the examples are Nickel-zinc ferrite ($NiZnFe_2O_4$), Manganese-zinc ferrite ($MnZnFe_2O_4$), Lithium Ferrite ($LiFe_5O_8$) [22–24].

2.2 Classification Based on Crystal Structure

Additionally, ferrites are categorized according to their crystal structure, which determines their characteristics and suitability for different uses. Spinel, garnet, hexaferrite, and orthoferrite are the main structural kinds which are illustrated in Fig. 1. Model crystal structures of spinel, garnet, hexaferrite, and orthoferrite ferrites, generated using VESTA software based on crystallographic data from standard references or from different cif file from COD(Crystallography Open Database) [25]. Because of their unique crystal structures, which determine their electrical and magnetic characteristics, each type can be used in a variety of technological applications.

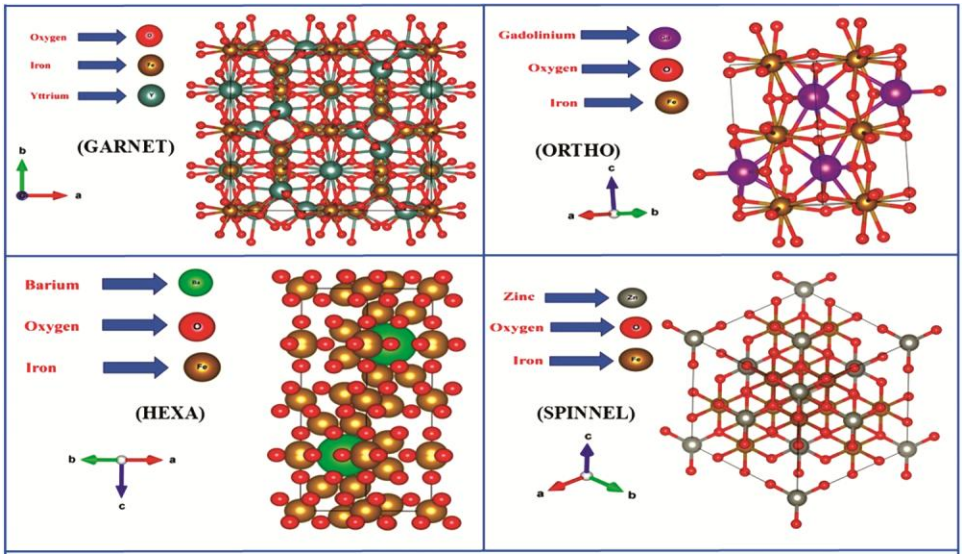

Fig. 1 — Model crystal structures of garnet, hexaferrite, orthoferrite, and spinel ferrites

2.2.1 Spinel Ferrites

With the general formula AB_2O_4, spinel ferrites have a cubic crystal structure. A stands for a divalent metal ion (like Ni^{2+}, Zn^{2+}, or Co^{2+}), and B for a trivalent metal ion (like Fe^{3+}). The metal cations occupy interstitial spaces, whereas the oxygen ions form a densely packed face-centered cubic lattice. Normal spinel and inverse spinel are the two primary structural topologies that result from the special cation arrangement found in spinel ferrites.

Normal Spinel

In a typical spinel structure, trivalent iron ions occupy the octahedral (B) sites, whereas divalent metal ions occupy the tetrahedral (A) sites[26-27]. The magnetic characteristics of zinc ferrite ($ZnFeO_4$), a common example of a normal spinel, are determined by the interactions between the iron ions on the octahedral sites. zinc ferrite($ZnFe_2O_4$) and magnesium ferrite ($MgFe_2O_4$) are examples of normal Spinel structure[28-29].

Inverse Spinel

An inverse spinel structure's tetrahedral (A) sites contain half of the trivalent iron ions, while the octahedral (B) sites contain the other half together with the divalent metal ions. Inverse spinel is common in cobalt ferrite ($CoFe_2O_4$) and nickel ferrite ($NiFe2O_4$)[30–32]. In this instance, the distribution of iron ions across both tetrahedral and octahedral sites results in more complicated magnetic interactions and improved magnetic characteristics[33–35].

Spinel ferrites are widely used in transformers, electromagnetic interference (EMI) suppression, and magnetic recording, among other applications. Their low eddy current losses and excellent electrical resistance make them perfect for high-frequency devices[36].

2.2.2 Garnet Ferrites

With the general formula $A_3B_5O_{12}$, garnet ferrites have a more complicated crystal structure than spinels. Trivalent rare earth ions (such Y^{3+}, Gd^{3+}, or Nd^{3+}) occupy the A sites in garnet ferrites, while trivalent iron ions (Fe^{3+}) occupy the B sites. Eight formula units make up a garnet ferrite's unit cell, which results in a sizable and complex crystal structure. Because of its superior magnetic characteristics and minimal magnetic damping, yttrium iron garnet ($YFeO_{12}$) is one of the most researched garnet ferrites and can be used in microwave and magneto-optical applications[37,38].

Because of their strong saturation magnetization and low loss magnetic behaviour, garnet ferrites are very useful in high-frequency applications. The garnet structure's magnetic anisotropy is further enhanced by the addition of rare earth ions, making it suitable for application in devices including circulators, magneto-optical modulators, and isolators[39-40].

2.2.3 Hexaferrites

Hexaferrites, sometimes referred to as hexagonal ferrites, are distinguished by their high saturation magnetization and strong coercivity and layered structure. Data storage, microwave devices, and permanent magnets all make extensive use of them. $MFe_{12}O_{19}$ is the typical formula for hexaferrites, where M stands for a divalent metal ion (such Ba^{2+}, Sr^{2+}, or Pb^{2+})[41-42].

Barium hexaferrite ($BaFe_{12}O_{19}$), one of the most investigated hexaferrites, has outstanding magnetic properties and is extensively used in permanent magnets and recording mediums. Hexaferrites' substantial magnetic anisotropy and high coercive force are due to its hexagonal crystal structure, which contains layered oxygen ions[43,44].

Hexaferrites' magnetic properties can be further improved by substituting rare earth ions, making them ideal for high-frequency and high-density data storage applications. Adding Nd^{3+} or La^{3+} to barium hexaferrite improves its magnetism and coercivity, making it ideal for advanced magnetic applications[45,46].

2.2.4 Orthoferrites

Orthoferrites are differentiated by their anisotropic magnetic properties and orthorhombic crystal structures. Orthoferrites are typically denoted as RFe_2O_3, with R representing a trivalent rare earth ion (e.g., La^{3+}, Nd^{3+}, or Sm^{3+}). Because of its high magnetic anisotropy and magneto-optical effects, orthoferrites are ideal for use in spintronic and magneto-optical devices[47–49].

Orthoferrites often exhibit minor ferromagnetism due to spin canting in their antiferromagnetic structure. This feature makes them ideal for use in memory devices and magneto-optical sensors. Rare earth ions can be introduced into the orthoferrite structure to significantly alter its magnetic behaviour, boosting spintronic applications and providing greater magneto-optical effects[50–52].

3 Specific Focus: Nickel Ferrite ($NiFe_2O_4$) and its Derivatives

Nickel ferrite ($NiFe_2O_4$) is a well explored soft ferrite with excellent magnetic, electrical, and dielectric properties[53]. The use of nickel ferrite in sensors, magnetic storage media, and high-frequency devices has sparked significant scientific interest[9-54-55]. This section will look at the oxygen position parameter, simulated X-ray diffraction (XRD) patterns of nickel ferrite, its structural features, and the impact of rare-earth doping in improving its properties[53]. Additionally, the discussion will briefly touch upon its derivatives, including nickel-zinc ferrite, nickel-zinc-copper ferrite, and nickel ferrite-based composites[56], highlighting their structural modifications and enhanced functionalities[57–59].

3.1 Importance of Nickel Ferrite

An inverse spinel ferrite, nickel ferrite (Chemical formula: $NiFe_2O_4$) has moderate magnetization, low eddy current losses, and high resistivity. Because of these characteristics, it can be used for a variety of purposes, such as:

- **Magnetic Storage Media:** Nickel ferrite's high magnetic saturation and low coercivity make it suitable for use in data storage devices and magnetic tapes, where the material needs to have strong but readily switchable magnetization[7].
- **High-Frequency Devices:** An appropriate core material for transformers, inductors, and antennas operating in the megahertz frequency range is nickel ferrite because of its high electrical resistivity, which reduces eddy current losses[60-61].
- **Magnetic Sensors:** Nickel ferrite is utilized in many magnetic field sensing applications, including Hall effect sensors and magneto-resistive devices, because of its soft magnetic characteristics and sensitivity to external magnetic fields[62-63].

Beyond these uses, nickel ferrite's significance in cutting-edge technological applications is further increased by its doping with rare earth elements, which allows for customization of its characteristics.

3.2 Crystal Structure of Nickel Ferrite

Nickel ferrite is classified within the inverse spinel structural category, where divalent nickel ions (Ni^{2+}) primarily occupy the octahedral (B) sites. In this structure, trivalent iron ions (Fe^{3+}) are distributed such that half occupy tetrahedral (A) sites while the other half are located in octahedral (B) sites. The oxygen anions (O^{2-}) form a face-centered cubic (FCC) lattice, with metal cations positioned in the interstitial sites[25].

In the context of the inverse spinel configuration:

- Tetrahedral sites (A sites) are occupied by Fe^{3+} ions.
- Octahedral sites (B sites) are shared between Ni^{2+} and Fe^{3+} ions.

The arrangement of cations in these interstitial sites significantly influences the magnetic and electrical properties of nickel ferrite. The magnetic moments of Fe^{3+} ions in both A and B sites exhibit anti-ferromagnetic interactions, while Ni^{2+} ions in the B sites contribute to the overall net magnetization [64-65]. Model Structure of Nickel ferrite with its tetrahedral and octahedral sites are displayed in Fig. 2.

Recent studies have shown that doping with rare-earth elements, such as terbium, can notably alter these properties. For instance, terbium doping results in a decrease in both saturation magnetization and coercivity, with saturation magnetization reaching a

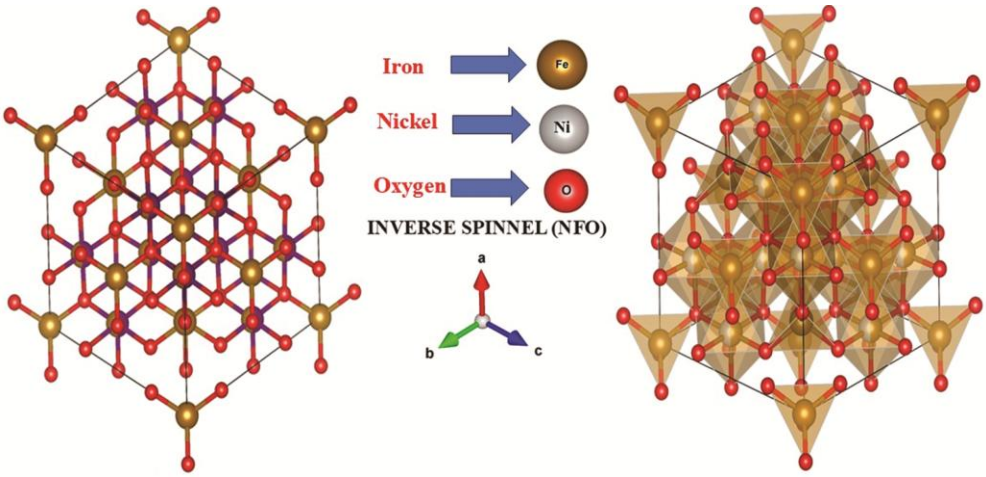

Fig. 2 — Crystal structure of pure nickel ferrite ($NiFe_2O_4$) showing octahedral and tetrahedral sites

minimum of approximately 30.6 emu/g at a doping level of 0.1[66], and the Curie temperature is reduced from 938 K to 899 K with increased terbium content.

Visualization tools like VESTA software facilitate the simulation of $NiFe_2O_4$'s structure, illustrating how Fe^{3+} and Ni^{2+} ions are arranged within the octahedral and tetrahedral sites. This simulated crystal structure is crucial for analysing cation distribution, oxygen positions, and how lattice distortions affect magnetic properties. Understanding this structure helps predict how modifications, such as rare-earth element doping, influence ferrite behaviour.

A typical representation of the simulated structure includes:

- Oxygen ions forming the lattice framework.
- Ni^{2+} ions occupying octahedral positions (B sites).
- Fe^{3+} ions distributed between tetrahedral (A sites) and octahedral (B sites).

The lattice parameters for $NiFe_2O_4$ have been reported to be around 0.8284 nm to 0.8322 nm depending on synthesis methods[67] . This information is essential for understanding the structural characteristics and optimizing the material's properties for various applications.

3.3 Simulated X-ray Diffraction (XRD) Pattern of Nickel Ferrite

The technique of X-ray diffraction (XRD) is crucial for analysing the crystal structure of materials, such as nickel ferrite. Distinct peaks, such as (220), (311), (400), (511), and (440), that correlate to the planes of its cubic spinel structure are commonly seen in the XRD pattern for $NiFe_2O_4$ as demonstrated in the simulated XRD pattern in Fig. 3. These peaks are essential for determining phase purity, lattice parameters, and crystallite size[68].

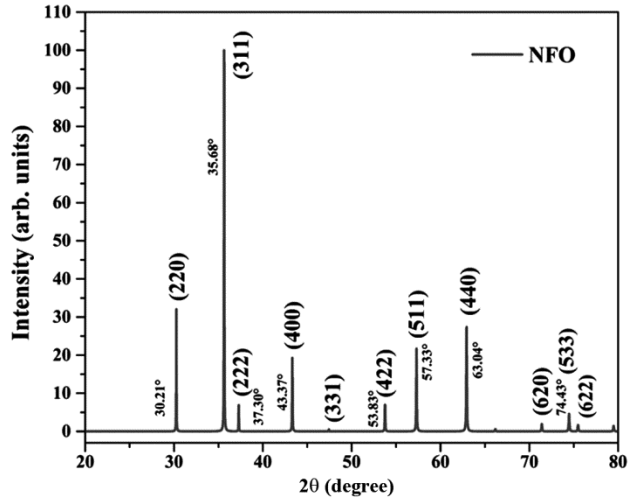

Fig. 3 — Simulated indexed XRD pattern of pure Nickel ferrite

Software like as VESTA can be used to create a simulated XRD pattern for pure nickel ferrite, which shows the relative intensities and distinctive peak positions linked to the spinel structure. The phase purity and crystallinity of the synthesized ferrite are often verified by comparing this simulated data with experimental XRD results[69].

The following parameters are commonly seen in the nickel ferrite XRD pattern:

- **Crystallite Size:** This is calculated from the broadening of diffraction peaks using the Scherrer equation.
- **Lattice Parameter (a_0):** This parameter is derived from the peak positions and provides insights into the unit cell dimensions of the spinel lattice.
- **Phase Purity:** The presence of secondary phases, such as Fe_2O_3, can be detected as additional peaks in the XRD pattern, indicating incomplete reactions or impurity phases [70-71].

In recent studies, doping was utilized to study changes in nickel ferrite properties. For example, zinc doping has been shown to have a significant effect on microstructural and magnetic characteristics. Studies reveal that substituting zinc ions for nickel ions increases the lattice properties while decreasing the crystallite size[24-72].

The crystallite size of nickel ferrite is traditionally estimated from the broadening of XRD peaks using the Scherrer equation, which provides a basic approximation based on size-induced broadening[68] . However, this method is limited as it does not account for lattice strain or instrumental effects. Modern approaches, such as the Williamson-Hall method, Rietveld refinement, or whole powder pattern modeling, offer more accurate and comprehensive analysis by considering both size and strain contributions, as well as phase purity and lattice parameters[73–75]. These methods are increasingly preferred in current research for precise structural characterization of ferrites.

In addition, gas sensing studies have revealed that in nickel zinc ferrite nanoparticles with zinc varying improves their sensitivity to hydrogen gas, resulting in a significant reaction at specific concentrations and temperatures[24].

An in-depth understanding of the structural study of nickel ferrite using X-ray diffraction techniques,

together with knowledge of the effects of doping, shows the material's potential applications in a variety of technological fields.

3.4 Oxygen Position Parameter in Nickel Ferrite

In spinel ferrites, the oxygen position parameter (u) refers to the displacement of oxygen anions from their ideal positions inside the lattice. This property has a significant influence on the distribution of cations and the magnetic interactions between ions within the lattice. Oxygen anions in nickel ferrite (NiFe2O4) typically form a close-packed structure; any deviation from this ideal location results in lattice distortion, which affects the material's electrical and magnetic properties.

There are two experimental ways for measuring the oxygen location parameter: neutron diffraction and synchrotron radiation. The oxygen parameter 'u' in nickel ferrites is not highly sensitive to the degree of inversion in the structure, as shown in studies of doped nickel ferrites [76]. Variations in oxygen stoichiometry affect the diffusion coefficients of oxygen, with higher contents leading to a diffusion coefficient independent of stoichiometry[77]. The oxygen parameter plays a vital role in enhancing the electrocatalytic activity for the oxygen evolution reaction (OER), where optimizing the lattice oxygen can improve performance significantly[78].

While the oxygen parameter is essential for enhancing the properties of nickel ferrites, it is also important to consider that excessive doping or alterations in stoichiometry can lead to structural instability, potentially diminishing the material's effectiveness in practical applications.

4 Influence of Rare Earth Incorporation in Nickel Ferrite ($NiFe_2O_4$)

Figure 4 demonstrates how Rare earth (RE) doping in nickel ferrite ($NiFe_2O_4$) causes structural changes that affect the material's electrical and dielectric properties. Nickel ferrite, a well-known inverse spinel structure, has attracted attention for its potential applications in a variety of electronic devices, sensors, and high-frequency components. The inclusion of rare earth ions causes modifications in resistivity, conductivity, and dielectric behavior in different ferrites, which are driven by changes in cation distribution and the formation of secondary phases[79-80]. In sol-gel or combustion synthesis, oxidants are typically metal nitrates (e.g., nickel nitrate, iron nitrate), providing oxygen for the reaction. Other

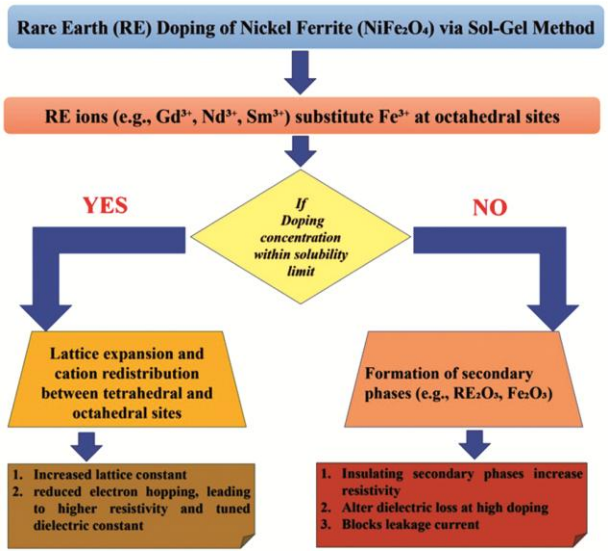

Fig. 4 — Flowchart showing rare earth-induced distortion, structural changes, and property modification in ferrites

oxidants like sodium perchlorate ($NaClO_4$) can be used, as seen in combustion synthesis studies[81].

4.1 Structural Impact of Rare Earth Doping

Incorporating rare earth (RE) ions like Gd^{3+}, Nd^{3+}, and Sm^{3+} into the nickel ferrite lattice alters its structural and physical properties due to their greater ionic radii compared to Fe^{3+} and Ni^{2+}. These RE ions preferentially occupy octahedral positions in the spinel structure, producing lattice expansion and changing the cation distribution between tetrahedral and octahedral sites. Such variations in lattice parameters and cation arrangement have an impact not only on the crystal structure but also on defect chemistry, which affects the material's electrical and magnetic properties. The concentration of RE dopants put into the ferrite matrix strongly influences the degree of lattice distortion and property alteration[82-83].

The solubility limit is an important aspect in RE doping because it limits the highest concentration of RE ions that may be homogeneously integrated into the nickel ferrite lattice without forming secondary phases. Beyond this limit, undesired phases including rare earth oxides (RE_2O_3) tend to precipitate, affecting the structural coherence and performance of the ferrite. Furthermore, the presence of large RE ions in the lattice inhibits crystallite growth during synthesis, resulting in smaller crystallites and different microstructural characteristics. This reduction in crystallite size can have an impact on grain boundary properties as well as electrical conductivity. As a result, a full understanding of the interaction between

RE doping concentration, solubility limits, and the consequent structural changes is required for adjusting nickel ferrite characteristics. Such optimization is particularly important for enhancing its applicability in various technological domains, including magnetic devices, catalysis, and sensors.

4.1.1 Below the Solubility Limit

When the RE ion concentration is within the solubility limit, the dopants successfully substitute for Fe^{3+} ions at the B sites, leading to lattice expansion and minor distortions, while maintaining a single-phase ferrite structure. The electrical properties in this regime can be fine-tuned through cation redistribution and changes in the lattice structure, which directly affect the conductivity and dielectric behaviour [84].

Lattice expansion

The introduction of RE ions, which are typically bigger than Fe^{3+} and Ni^{2+}, increases the lattice constant. This expansion is visible in X-ray diffraction (XRD) patterns, as diffraction peaks move to lower angles due to the enlargement of the unit cell. The higher lattice constant also affects charge carrier mobility and the electron hopping distance between cations, which has a strong influence on the material's electrical conductivity [5-16]. A higher lattice constant increases the distance between cations (e.g., Fe^{2+} and Fe^{3+}), lengthening the electron hopping distance. This reduces charge carrier mobility, as electrons must travel farther, potentially decreasing conductivity. In doped ferrites, lattice expansion from RE ions can further disrupt hopping, increasing resistivity [85]for this effect, noting how lattice changes impact carrier mobility.

Cation Redistribution

In nickel ferrite, rare earth (RE) doping causes notable changes in the distribution of cations between the spinel structure's tetrahedral (A) and octahedral (B) sites. These cations may redistribute when RE ions are added, as they usually have a higher ionic radius than Ni^{2+} and Fe^{3+}. Ni^{2+} and Fe^{2+} ions, in particular, may move between sites A and B to provide room for the structural tension brought on by RE incorporation. Electron hopping between Fe^{2+} and Fe^{3+} ions at B-sites is the basic charge transport mechanism in ferrites that is impacted by this redistribution. These hopping pathways can become interrupted by changes in site occupancy, which can alter electrical conductivity. RE ions may also partially fill the lattice's interstitial spots. The electrical structure and conductivity of the material are further influenced by the local lattice distortions introduced by this occupation. The ionic radius, valence, and solubility limit of the particular RE element being utilized determine how much of these changes occur. The surplus RE ions separate into secondary phases, which will be covered in more detail in the next section, after reaching a critical concentration[15,16,86].

4.1.2 Beyond the Solubility Limit

When the concentration of RE ions exceeds the solubility limit, secondary phases such as rare earth oxides (RE_2O_3) and iron-rich oxides (Fe_2O_3) begin to precipitate. These secondary phases, which are typically insulating, contribute to increased resistivity. The formation of secondary phases is typically confirmed by XRD patterns, where additional peaks appear corresponding to the RE oxide phases. This indicates a structural evolution within the material as the excess RE ions are no longer incorporated into the ferrite matrix but instead form separate phases [85].

The generation of these phases depends on the ionic radius of the RE ions and their charge compatibility with the Fe^{3+} ions they replace at the B sites. While secondary phases might reduce electrical conductivity due to their insulating nature, they can also bring unique microstructural properties that may benefit specific applications. To attain the desired material properties, the doping concentration can be carefully adjusted to balance the advantages provided by both the primary ferrite phase and the secondary phase [16].

4.2 Factors Influencing the Phase Formation in Rare Earth Doped Nickel Ferrite In Sol Gel Auto Combustion Method

The synthesis process plays a crucial role in achieving a pure nickel ferrite phase, with the occasional formation of secondary phases when doped with RE ions, thereby influencing its various properties. Among the available approaches, the sol-gel auto combustion process has a substantial effect on dopant distribution, microstructure, grain size, porosity, and phase purity. Secondary phases, including rare earth oxides (RE_2O_3) and iron oxides (Fe_2O_3), can alter the material's electrical transport and dielectric characteristics. Model structures of doped nickel ferrite and the secondary phase are illustrated in Fig. 5. XRD pattern of the bi-phase nickel ferrite is shown in Fig. 6 where the secondary orthorhombic phases are shown in asterisk (*). X-ray diffraction (XRD) determines crystallinity in

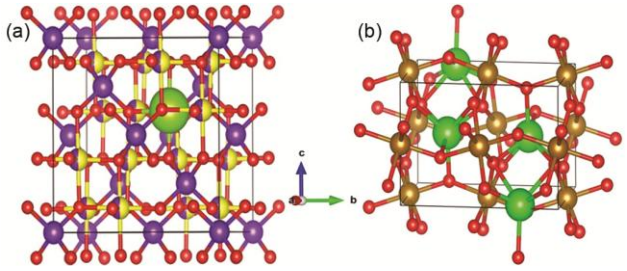

Fig. 5 — Crystal structures of Rare earth substituted (a) Nickel ferrite along with (b)secondary orthorhombic phase

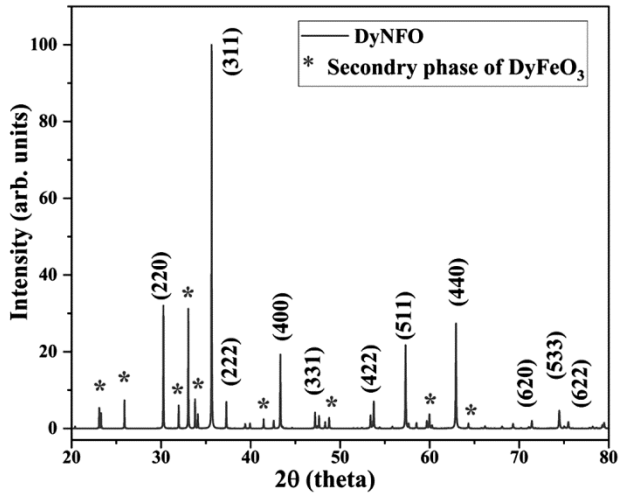

Fig. 6 — Simulated XRD pattern of Bi-phase doped ferrite

nickel ferrite mostly by analyzing peak sharpness, intensity, and the number of different reflections. Sharper and more powerful peaks in the 2θ range of 20°-80° indicate improved long-range atomic order and larger crystallite sizes, indicating higher crystallinity. This is quantified using the Scherrer equation, where a decrease in full width at half maximum (FWHM) indicates crystallite development.

The sol-gel auto combustion method is a sophisticated and frequently used technology for creating metal oxides and nanomaterials, such as ferrites. To make a sol, metal precursors are first dissolved in a solvent, which is usually accompanied by an oxidant and a fuel. When heated, the sol undergoes auto-combustion, quickly creating a porous gel and releasing gases. This exothermic reaction streamlines the synthesis process and results in homogeneous nanoparticles with regulated shape. Following calcination, the final product has increased stability and crystallinity, which provides numerous important advantages for controlling doping and phase formation. Following are two noteworthy benefits of this process:

4.2.1 Enhanced Control Over Doping and Phase Formation

The sol-gel process is well known for its ability to achieve homogeneous dopant dispersion inside the nickel ferrite lattice, which includes the integration of rare earth (RE) elements. This approach allows for exact control of doping concentrations, which reduces the chance of large-scale secondary phase formation. However, when RE concentrations reach the solubility limit of nickel ferrite, secondary phases such as RE oxides can develop, which are often finer dispersed than those produced by traditional methods[5-16]. Controlled doping and phase formation can be refined further by optimizing critical synthesis parameters: keeping the solution pH around 6 ensures homogeneous precursor distribution; selecting appropriate combustion agents (e.g., citric acid, urea) regulates reaction temperature and improves phase purity; and ensuring accurate precursor stoichiometry, as well as precise control over calcination temperature and time, is critical for single-phase spinel formation. The sol-gel process, combined with careful synthesis condition adjustment, allows for homogeneous dopant inclusion and suppression of secondary phases, keeping nickel ferrite's ideal structural, magnetic, and electrical properties[83].

4.2.2 Fine Grain Structure

The sol-gel process often yields materials with larger surface areas, smaller particle sizes, and increased porosity, as the rapid combustion and gas release during synthesis promote fine grain structures and high surface area nanoparticles[87–89]. Grain boundaries in smaller grains serve as charge carrier dispersion sites, often resulting in higher electrical resistivity. Furthermore, the porosity found in sol-gel-derived ferrites can trap rare earth dopants at grain boundaries, favouring the production of secondary phases[5].

In the sol gel auto combustion method, two controlling parameters have reportedly influenced the appearance of the secondary orthorhombic phase massively. One is pH level and the other is the combustion agent.

4.3 Role of pH Value Maintenance in the Phase Formation of Ferrite

Ferrites' structural characteristics and phase development are greatly influenced by the pH level at which they are synthesized. Maintaining a pH of about 6 has been found to be ideal for obtaining desired

properties in the context of rare earth-doped ferrites produced using the auto-combustion sol-gel process[90].

Lower pH values, especially below 4, promote hematite (α-Fe2O3) formation, hindering the transition to the desired spinel ferrite phase. When the pH climbs to around 6, the synthesis begins to favour the formation of spinel ferrites [91]. This transition is important because it impacts the final material's magnetic properties as well as the size of the crystallites. For example, research shows that ferrite samples produced at pH 6 have stronger crystallinity and optimal magnetic behaviour than those produced at lower or higher pH [90].

Particle morphology can also alter as a result of pH variations. In order to get similar magnetic characteristics across the sample, a more uniform particle dispersion is seen at pH values close to 6[92]. Because of the balanced ion concentration and reactivity at this pH level, the synthesis process is more easily controlled.

Changes in crystallite sizes and lattice properties can also be connected to the effect of pH on structural features. For instance, because of excessive ion reactivity and phase segregation, raising the pH above 6 may result in bigger crystallite sizes and changed lattice properties[91]. This implies that in order to maximize the structural integrity and functional characteristics of rare earth-doped ferrites, precise pH regulation is required.

4.4 Role of Combustion Agent in the phase Formation of Ferrite

In the sol-gel auto-combustion process, the combustion agent used has a significant effect on the synthesis and characteristics of rare earth-doped ferrites. Combustion agents such as maleic acid, urea, and citric acid not only provide the heat needed to create spinel ferrites, but they also greatly stabilize metal cations throughout the synthesis process[87-88].

The combustion agent helps metal cations in forming stable complexes during the auto-combustion process, preventing selective precipitation caused by water evaporation. This stabilization is required to ensure a homogenous distribution of metal ions in the final ferrite structure. The crystallinity and shape of the synthesized ferrites can be greatly modified by the type of combustion agent used. Using urea as a combustion agent, for example, has been shown to result in lower degrees of crystallinity than citric acid or maleic acid, which create clear, sharp peaks in X-ray diffraction (XRD) patterns, indicating high crystallinity [88].

The type of fuel and its proportion of metal cations are two variables that can influence the complex combustion process. The microstructure and functional properties of ferrite materials are influenced by ideal temperature conditions and full combustion, which necessitate a proper balance of these components. For example, it has been shown that using different chelating agents, such as citric acid, urea, or maleic acid, generates changes in the magnetic properties of ferrites, with certain agents (e.g., citric acid) encouraging higher coercivity and magnetization values due to improved crystallinity and cation distribution[88-93].

In addition, advances in microwave-assisted combustion methods have demonstrated that employing microwave radiation can enhance combustion efficiency, leading in improved phase purity and faster synthesis times [89]. This method allows for faster heating and greater control over particle agglomeration, resulting in high-quality ferrite nanoparticles [94].

4.5 Role of Sintering Temperature in Phase Formation and Properties

The sintering temperature is an important parameter in the sol-gel auto-combustion synthesis of rare earth-doped nickel ferrites, influencing phase purity, crystallite size, and functional characteristics. Optimal sintering temperatures (600-1000°C) increase spinel production while reducing secondary phases like Fe_2O_3 or RE_2O_3 [95]. Higher temperatures promote crystallinity and grain development, which reduces porosity and increases crystallite size, potentially lowering electrical resistivity due to enhanced charge carrier mobility[50]. However, high sintering temperatures can cause phase segregation or loss of volatile components, reducing magnetic and dielectric characteristics. For example, research on Gd-doped nickel ferrites demonstrate that sintering at 800°C maximizes phase purity and magnetic saturation, but higher temperatures (>1000°C) cause secondary phase development. Careful control of sintering temperature is thus essential to balance structural integrity and functional performance in RE-doped ferrites.

5 Review of Tailored Transport Properties upon RE Doping

Rare earth doping in nickel ferrite has a major effect on transport parameters such as electrical

conductivity and charge carrier mobility. RE doping alters charge carrier hopping between Fe^{2+} and Fe^{3+} ions, leading to structural alterations and changes in cation vacancy concentrations, according to several studies. The following highlights the main alterations observed in transport characteristics as a result of RE doping: -

5.1 Polar on Hopping Mechanism

Electrical conduction in ferrites involves polaron hopping, where Fe^{2+} and Fe^{3+} ions exchange electrons across nearby oxygen atoms. RE doping disrupts this process by altering the local crystal field and introducing defects that limit polaron mobility[5]. As a result, the material's conductivity drops as the RE doping concentration increases, particularly when secondary phases occur [16].

5.2 Small Polaron Hopping

Involves localized charge carriers strongly coupled to lattice distortions, resulting in short-range hopping. This is common in ferrites due to strong electron-phonon interactions, leading to lower mobility and higher activation energy. Small polaron hopping is often dominant in RE-doped ferrites, where lattice distortions from larger RE ions further localize carriers[95-96].

5.3 Large Polaron Hopping

Involves less localized charge carriers with weaker lattice interactions, allowing for longer-range transport. This is less common in ferrites but may occur in systems with reduced lattice distortions or specific doping conditions.

5.4 Electrical Resistivity

Rare earth (RE) doping in nickel ferrite plays a crucial role in tuning transport properties such as electrical resistivity and conductivity. These properties are significantly influenced by structural modifications induced by RE dopants, including lattice distortions, cation vacancy concentrations, and the formation of secondary phases. Depending on the application, RE doping can either increase the resistivity for enhanced insulation or decrease it to improve conductivity, making RE-doped nickel ferrite versatile for various technological applications.

Incorporating RE ions with greater ionic radii than Fe^{3+} or Ni^{2+} might cause unit cell expansion and alter electron hopping mechanisms between Fe^{2+} and Fe^{3+} ions, affecting conduction behavior. This tunability is especially useful in applications like as magnetic sensors, microwave devices, and energy storage systems, where precise electrical performance is required. Recent studies also indicate that RE doping can improve thermal stability and reduce dielectric losses, thus increasing the overall efficiency of ferrite-based components[97].

6 Electrical Resistivity and Conductivity

RE doping has been widely reported to increase the electrical resistivity of nickel ferrite due to the introduction of lattice distortions. Larger RE ions disrupt the regular lattice, impeding the polaron hopping mechanism between Fe^{2+} and Fe^{3+} ions, which is the primary charge transport mechanism. Moreover, the formation of secondary phases, such as rare earth oxides, further enhances resistivity as these phases are generally insulating. For instance, Gd-doped nickel ferrite has been shown to exhibit significantly higher resistivity, making it suitable for applications requiring reduced eddy current losses [95]. In addition to increased resistivity, RE doping influences microstructural morphology by increasing grain boundary resistivity and grain size, both of which contribute to the reduction of charge carrier mobility. This leads to enhanced performance in high-frequency applications like transformer cores and EMI shielding. Furthermore, investigations have revealed that RE doping not only alters electrical behavior, but also improves thermal stability and minimizes dielectric losses, widening the operational reliability of these materials under diverse environmental circumstances[98].

P. Venkata Srinivasa Rao *et al*., (2018) reported that Gd doping in Ni-Cu-Zn ferrites led to increased resistivity values up to 9.5×10^{7} Ω·m at a concentration of x=0.12, showing that RE doping can effectively enhance resistive properties [99]. Similarly, Farid *et al*., (2015) study reveals that doping Neodymium (Nd) ions with Nickel-Cobalt ferrites leads to an increase in the direct current (DC) resistivity of the material, the resistivity increases with higher Nd concentrations, indicating that the material becomes less conductive as more Nd is added. This is primarily due to the larger ionic radius of Nd compared to the ions it replaces, which affects the movement of charge carriers within the ferrite structure[100].

However, RE doping can also be used to reduce resistivity, effectively increasing conductivity in certain cases. For example, Dwevedi et al., (2009) observed that pure Ni ferrite exhibits the highest resistivity and conductivity values, while the rare Earth-doped compounds show lower resistivity and,

consequently, higher conductivity. This change is attributed to the structural modifications and the increased hopping of charge carriers due to the presence of rare Earth ions [101]. Almessiere *et al*. observed that incorporating Ce^{3+} and Dy^{3+} ions into NiCo ferrite significantly alters both AC and DC conductivity, underscoring the role of rare earth doping in modifying the electrical properties of ferrites and influencing their conduction mechanisms. electrrical properties of ferrite materials, which ultimately affects the conduction mechanisms within the material [102]. Additionally, Sinha et al., (2018) reported that Doping Gd into nickel ferrite affects its electrical conductivity significantly. The study found that the ac conductivity of the samples increases with the increase in Gd doping concentration up to 10% (x = 0.10) and then decreases at higher concentrations (x = 0.15) [103].

The flexibility offered by RE doping makes it possible to adjust resistivity and conductivity for specific applications. Whether the goal is to increase resistivity for insulating purposes or to reduce it for better conductivity, the controlled introduction of RE dopants allows fine-tuning of transport properties based on the desired application.

6.1 Thermal Activation Energy

The introduction of rare earth elements has been shown to increase the energy barrier for charge carrier movement, thus elevating the thermal activation energy of the material. Guragain *et al*., (2020) study reveals that effect of terbium ion substitution in inverse spinel nickel ferrite results reductions in Curie temperature and alterations in magnetic properties suggest that doping can have a significant impact on thermal activation processes in nickel ferrite[84]. Rezlescu et al., (1997) reported that R_2O Tb^{3+} (R = Yb, Er, Dy, Tb, Gd, Sm and Ce) doping in nickel zinc ferrite increase the thermal activation energy at elevated temperatures is due to the thermal activation of carrier mobility, which is sensitive to the microstructure of the material [104]. Additionally, Sowjanya *et al*., (2023) found that multi rare earth element doped Ni–Co ferrite enhanced the lattice parameter of the doped ferrite increased from 8.218 Å to 8.243 Å due to doping, which could imply changes in the thermal properties, including activation energy [105]. Phugate *et al*., (2020) reported that the introduction of Ho^{3+} ions into the Co–Ni ferrite matrix affects the thermal properties of the material. As the concentration of Ho^{3+} ions increases, the thermal activation energy is likely to change due to alterations in the crystal structure and cation distribution within the ferrite [106].

6.2 Carrier Mobility

The mobility of charge carriers is also influenced by the size and valence state of the doped rare earth ions. Kumar *et al*., (2024) investigates that the doping of nickel ferrites with Ho, Gd, and La significantly influences the mobility of charge carriers by altering structural characteristics, enhancing conduction mechanisms, and reducing leakage current, which collectively contribute to improved electrical performance [92]. In another study, Nag *et al*,. (2019) found that doping nickel zinc ferrite with Er^{3+} ions leads to significant changes in the mobility of charge carriers, particularly at an optimal concentration of x=0.025, which enhances the material's dielectric properties and suitability for high-frequency applications [107]. Additionally, Almessiere *et al*., (2021) demonstrated that the introduction of Ce^{3+} and Dy^{3+} ions into the Ni–Co ferrite structure affects the charge carrier mobility. The study indicates that the ac conductivity measurements confirmed a power-law relationship, which is largely dependent on the Ce–Dy content. This suggests that the mobility of charge carriers is influenced by the concentration of these dopants [102]. Finally, Srinivasamurthy *et al.,* (2018) reported that doping with Ce^{3+} ions in Co-Ni ferrites affects the charge carrier mobility significantly. The introduction of Ce^{3+} ions replaces some of the Fe^{3+} ions in the ferrite structure, which influences the hopping mechanism of charge carriers. This is because the mobility of charge carriers is often linked to the ability of electrons to hop between different oxidation states of iron ions (Fe^{2+} and Fe^{3+}) in the ferrite matrix[108].

7 Review of Modified Dielectric Properties upon Rare Earth (RE) Doping

The dielectric properties of ferrites are highly dependent on microstructure, grain size, and the presence of secondary phases. Rare earth (RE) doping introduces significant modifications to these properties. The following summarizes the key changes in dielectric properties observed due to RE doping:

7.1 Dielectric Constant

When nickel ferrite is doped with RE, its dielectric constant usually drops. This is due to the fact that the presence of RE ions suppresses the hopping of charge

carriers between Fe^{2+} and Fe^{3+} ions, which aids in material polarization. A drop in the dielectric constant results from the bigger RE ions' reduction of the quantity of charge carriers and obstruction of their motion. Nd-doped nickel ferrite, for instance, has demonstrated a lower dielectric constant than undoped ferrite, especially at higher frequencies[5-91].

In many cases, RE doping leads to a reduction in the dielectric constant because the hopping of charge carriers (Fe^{2+}/Fe^{3+}) is hindered by RE ions, resulting in decreased polarization. For example, the structural alterations brought about by doping cause the dielectric constant of neodymium-substituted copper nickel ferrite to decline with increasing frequency and attain a constant value at higher frequencies[109].

Conversely, some RE dopants can increase the dielectric constant due to the lattice distortion they introduce and the polarizability of RE ions, The study by Atta *et al*. (2021) examines how terbium (Tb3+) doping affects the dielectric characteristics of nickel ferrite (NFO) nanoparticles. The addition of Tb ions was shown to dramatically boost the dielectric constant. This improvement is explained by the material's enhanced polarization effects brought about by the rare-earth ions. This implies that doping with Tb3+ improves the material's electrical energy storage capacity, which is an essential characteristic for a variety of electronic applications[66]. Nag *et al.* (2019) similarly observed that Er^{3+} doping in nickel-zinc ferrite raised the dielectric constant to approximately 35 at 1 kHz [107]. Additionally, Atta *et al*., (2020) reported that a significant enhancement in the dielectric constant is observed due to the doping process. Specifically, the dielectric constant reaches a high value of 360 at a temperature of 303 K. This increase is attributed to the presence of Tb^{3+} ions in the NFO nanoparticles, which contribute to improved polarization effects within the material and this makes the material suitable for applications in electronic devices, particularly in capacitors and storage devices[110].

Ditta *et al*., reported that the dielectric constant of Gd and Dy co-doped Ni-Co ferrites decreases with increasing frequency, showing significant variations between low and high-frequency regions, influenced by polarization effects and electron dynamics [111]. Similarly, Bharathi and her teammates research indicates that the dielectric constant can increase by an order of magnitude with the substitution of Ho ions, highlighting the significant impact of these rare-earth elements on the electrical properties of Ni ferrites [112].

7.2 Dielectric Loss

Dielectric loss is the amount of energy released as heat in a dielectric substance when exposed to an alternating electric field. Dielectric loss in RE-doped ferrites typically reduces with doping, especially at higher frequencies. This is because reduced charge carrier mobility reduces polarization-induced energy dissipation. However, at very high doping levels, the creation of secondary phases may increase dielectric loss due to increased scattering and flaws in the material[107,108,113].

The reduction in dielectric loss with RE doping is often due to the inhibition of charge carrier motion, which is especially prominent at higher frequencies. Rajenimbalkar et al. (2024) reported that Ti-Zn co-doped nickel ferrites exhibited a significant decrease in dielectric loss, reaching as low as 0.02 at higher frequencies, indicating improved energy storage capabilities[85].

Nag *et al.* (2019) investigation indicates that the sample with 2.5% erbium doping (x=0.025) exhibited a relatively lower dielectric loss compared to the undoped nickel zinc ferrite. This suggests that the incorporation of Er^{3+} ions improves the dielectric performance of the ferrite. These enhancements are crucial for advancing the material's application in high-frequency electronic devices[107].

Luo *et al.,* (2017) research found that the dielectric loss tangent peaks at a doping concentration of x = 0.008, indicating a significant change in dielectric behavior due to Nd3+ ion doping in Ni–Zn ferrites, while lower and higher concentrations lead to a decrease in dielectric loss, the dielectric constant and dielectric loss tangent were measured across different concentrations of Nd^{3+} ions, specifically from 0.002 to 0.010[114]. Srinivasamurthy et al., (2018) studies found that the dielectric loss decreases with increasing frequency. At low frequencies, the dielectric loss is high because a large number of dipoles can align with the electric field, leading to significant energy loss. However, as the frequency increases, the ability of dipoles to follow the rapidly changing field diminishes, resulting in lower dielectric loss. This behavior aligns with Debye's relaxation phenomena, where the dielectric loss decreases as the frequency increases [108].

7.3 Frequency Dependence

The dielectric characteristics of RE-doped nickel ferrite are extremely frequency dependant. At low frequencies, space charge polarization causes charges to accumulate at grain boundaries and other imperfections, resulting in a high dielectric constant. However, at higher frequencies, the material's dipoles cannot keep up with the rapid fluctuations in the applied electric field, resulting in a reduction in the dielectric constant. RE doping alters this frequency dependence, making the material acceptable for specific frequency ranges in electronic applications including microwave devices and RF circuits[11 5].

Nag *et al.* (2019) found that the frequency dependence analysis demonstrated that the erbium-doped nickel zinc ferrite, especially with 2.5% doping, has promising dielectric properties that make it suitable for advanced electronic applications [107]. According to Ranga *et al.* (2023) The dielectric constant decreases with increasing frequency and La3+ ion concentration, while dielectric loss increases with temperature. These changes indicate that La3+ substitution affects the frequency dependence of dielectric properties in nickel ferrite nanoparticles[113]. Awati *et al*. (2021) found that the dielectric constant of the Tb3+ doped NiCuZn ferrites exhibits a dispersion behavior, which aligns with the Maxwell-Wagner model. This model explains how dielectric materials can show different dielectric constants at different frequencies due to the presence of multiple polarization mechanisms within the material [115]. Paswan *et al.* (2023) examined the dielectric relaxation (100 Hz–1 MHz), showing a higher dielectric constant in rare earth (La3+ and Sm3+) substituted samples than in pure nickel ferrite. AC conductivity was lower in substituted samples, exhibiting frequency-dependent electrical transport. Temperature-dependent analysis via Jonscher's power law indicated small polaron hopping below 200 °C, transitioning to correlated barrier hopping above this temperature[116].

8 Applications of RE-Doped Nickel Ferrite

RE-doped nickel ferrites are ideal for a variety of high-frequency and high-resistivity applications due to their superior electrical and dielectric properties. These benefits are due to changes in ionic distribution and structural modifications caused by rare earth doping.

Several key applications benefit from these enhanced properties:

- **High-Frequency Transformers and Inductors:** RE-doped nickel ferrite is suitable for use in high-frequency transformers, inductors, and other passive electronic components that require low eddy current losses due to its higher resistivity and reduced dielectric loss[117].
- **Capacitors and Resonators:** RE-doped nickel ferrites outperform capacitors and resonators in radio frequency and microwave circuits due to their lower dielectric loss and controllable dielectric constant[118].
- **Electromagnetic Interference (EMI) Suppression:** RE-doped ferrites are ideal for EMI suppression applications due to their increased resistivity and tuneable dielectric properties, which enable them to absorb and scatter unwanted electromagnetic signals[119 120].
- **Magnetic Data Storage:** The unique magnetic properties of RE-doped nickel ferrites make them ideal for use in magnetic data storage devices that require strong coercivity and heat stability[120].
- **Biomedical Applications:** Nickel ferrites magnetic properties, which may be altered by rare earth doping, have led to their use as MRI contrast agents and as a hyperthermia treatment[121].
- **Catalysis:** Rare earth-doped nickel ferrites have excellent catalytic properties, making them suitable for applications such as heterogeneous catalysis in environmental remediation methods[122].
- **Energy Storage Devices:** RE-doped nickel ferrites are intriguing materials for energy storage systems due to their high resistivity and low losses, which will aid in the development of more efficient power supply solutions[123].

9 Conclusion

To summarize, rare earth (RE) doping can significantly improve the electrical characteristics of nickel ferrite ($NiFe_2O_4$), which is crucial for advanced technological applications. This review has shown that the addition of RE components like Gd, La, Nd, and Sm causes significant modifications in the material's structure and performance. RE doping alters electron hopping dynamics between Fe^{2+} and Fe^{3+} ions, leading to higher resistivity and enhanced dielectric properties. Excessive doping can cause the production of secondary phases such as RE_2O_3, which can negatively affect electrical behaviour.

The synthesis process chosen is also important; techniques such as sol-gel and combustion offer greater control over phase purity and microstructure than standard solid-state procedures. Overall, while rare earth doping offers a diverse way to enhancing the electrical characteristics of nickel ferrite, striking the right balance between increased performance and secondary phase minimization remains a significant problem. Future research should concentrate breakthroughs in synthesis procedures in order to optimize the benefits of rare earth-doped nickel ferrites in functional devices.

Reference

1 Manhas A, Singh M, Hussain M I, Javed Y & Sharma S K, 2021, 1, doi:10.1007/978-3-030-79960-1_1.
2 Bharadwaj S & Kalyana Lakshmi Y, *Springer Nature link*, 2023, 17.
3 Kumari N, Kour S, Singh G & Sharma R K, *AIP Conf Proc*, 2020, 020164.
4 Youssef M, *Ferrites, Theory and Applications*, 2017.
5 Saha S & Routray K L, 2024, doi:10.21203/rs.3.rs-4252875/v1.
6 Wang G, Ma Z, Zheng Y, Cheng L, Xing H & Li Z, *RSC Adv*, 1452 (2024) 38345, doi:10.1039/D4RA06136E.
7 Asha, Juglan K C & Jain A, In 2024, 030127, doi: 10.1063/5.0192528.
8 Sowjanya P, Thirupathi G, Kumar M S, Ramesh T, Reddy M V R, Chelvane A, *et al.*, *J Alloys Compd*, 2024, 971172623, doi: 10.1016/j.jallcom.2023.172623.
9 Rana G, Dhiman P, Kumar A, Vo D V N, Sharma G, Sharma S, *et al.*, *Chem Eng Res Des*, 2021, 175182, doi:10.1016/j.cherd.2021.08.040.
10 Khan S N, Mir A, Manzoor S & Raees R, *Mater Chem Phys*, 2024, 320129378, doi: 10.1016/j.matchemphys.2024.129378.
11 Wang C, Zou B, Wu Y, Lu Z, Li Z, Xie D, *et al.*, *Phys Lett A*, 2024, 506129476,doi: 10.1016/j.physleta.2024.129476.
12 Routray K L & Saha S, *Phys Scr*, 995 (2024) 055950, doi: 10.1088/1402-4896/ad3ae0.
13 Praveen H & Chandran V G, *J Mater Sci Mater Electron*, 3418 (2023) 1446, doi: 10.1007/s10854-023-10884-y.
14 Praveen H & Girish Chandran V, *J Thermoplast Compos Mater*, 2025, doi: 10.1177/08927057251322172.
15 Šiljegović M, Cvejić Ž, Jankov S, Toth E, Herceg D, Odry P, *et al.*, *Electronics*, 138 (2024)1496, doi: 10.3390/electronics13081496.
16 Kumar S, Mondal C, Dutta A & Sinha A, *ECS J Solid State Sci Technol*, 137 (2024) 073017.
17 Materials Research Forum LLC, 2023, (Materials Research Foundations) 142, doi: 10.21741/9781644902318.
18 Jotania R, *ChemInform*, 2015, 4610, doi: 10.1002/chin.201510296.
19 Kumar S, Supriya S, Pandey R, Pradhan L K & Kar M, In 2018, 130040, doi: 10.1063/1.5029110.
20 Kools F, In concise encyclopedia of advanced ceramic materials, Elsevier, 1991, 200, doi: 10.1016/B978-0-08-034720-2.50059-9.
21 Koledintseva M Y, In 2018 IEEE symposium on electromagnetic compatibility, signal integrity and power integrity (EMC, SI & PI) IEEE; 2018, 1, doi: 10.1109/EMCSI.2018.8495248.
22 Petrescu LG, Petrescu MC, Ioniță V, Cazacu E & Constantinescu C D, *Materials (Basel)*, 2019, 1219, 3173, doi: 10.3390/ma12193173.
23 Ahmad Z, Khan S, Waqar S, Maqsood R & Ali Z A, *IEEE Trans Magn*, 5811 (2022) 1, doi: 10.1109/TMAG.2022.3204411.
24 Thakur P, Taneja S, Chahar D, Ravelo B & Thakur A, *J Magn Magn Mater*, 2021, 530167925, doi: 10.1016/j.jmmm.2021.167925.
25 Tsukimura K, Sasaki S & Kimizuka N, *Jpn J Appl Phys*, 366R (1997) 3609, doi: 10.1143/JJAP.36.3609.
26 Gogoi B & Das U, *Adv Mater Res*, 2023, 117679, doi: 10.4028/p-5bb090.
27 Tatte T R, *Int J Sci Res*, 1212 (2023) 605, doi: 10.21275/SR231204160235.
28 Silva F G da, Depeyrot J, Campos A F C, Aquino R, Fiorani D & Peddis D, *J Nanosci Nanotechnol*, 198 (2019) 4888, doi: 10.1166/jnn.2019.16877.
29 Gogoi B & Das U, 2022, doi:10.21203/rs.3.rs-2034802/v1.
30 Kumar V, Sarkar K, Kumar S, Srivastava R & Kumar R, *Int Res J Adv Eng Hub*, 206 (2024) 1659, doi:10.47392/IRJAEH.2024.0228.
31 Choi J, Kim D, Hong S J, Zhang X, Hong H, Chun H, *et al.*, *Appl Catal B Environ*, 2022, 315121504, doi: 10.1016/j.apcatb.2022.121504.
32 EL Maazouzi A, Masrour R & Jabar A, *J Supercond Nov Magn*, 3312 (2020) 3871, doi: 10.1007/s10948-020-05515-0.
33 Mund H S, Tiwari S, Sahariya J, Itou M, Sakurai Y & Ahuja B L, *J Appl Phys*, 2011, 1107, doi: 10.1063/1.3650251.
34 Wu J, Li N, Xu J, Jiang Y, Ye ZG, Xie Z, *et al*., *Appl Phys Lett*, 2011, 9920, doi: 10.1063/1.3662840.
35 Kim K J, Kim M H & Kim C S, *J Magn*, 192 (2014) 111, doi: 10.4283/JMAG.2014.19.2.111.
36 Zhao S, Wang C & Zhong B, *J Magn Magn Mater*, 2020, 495165753.
37 do Carmo J V C, de Cássia F Bezerra R, Guerra Y, Peña-Garcia R, Oliveira A C, Padron-Hernandez E, *et al.*, *Catalysts*, 129 (2022) 1033, doi: 10.3390/catal12091033.
38 Hu Y, Liu X S, Feng S J & Zen L, (2023), doi: 10.2139/ssrn.4510160.
39 Sharma A, Dipesh, Mahajan H & Srivastavaa AK, In 2024. p. 174–86, doi: 10.4018/979-8-3693-1306-0.ch008.
40 Sharma A & Dipesh, *Mater Perform Charact*, 131 (2024) 1, doi: 10.1520/MPC20230082.
41 Koutzarova T, Kolev S, Krezhov K, Georgieva B, Ghelev C, Cholakov T, *et al.*, *J Chem Technol Metall*, 594 (2024) 985, doi: 10.59957/jctm.v59.i4.2024.29.
42 Himanshi, Jasrotia R, Prakash J, Verma R, Thakur P, Kandwal A, *et al.*, *Phys B Condens Matter*, 2023, 667415202, doi: 10.1016/j.physb.2023.415202.
43 Gunanto YE, Sitompul H, Izaak MP, Jobiliong E, Yunasfi Y, Setiawan J, *et al.*, *Phys Scr*, 992 (2024) 025002, doi: 10.1088/1402-4896/ad1799.
44 Ahmed M R, Ibrahim E M M, Hamazaoui A, Rayan A M, Azab A A & Abdel Hakeem A M, *Phys Scr*, 9911 (2024) 115905, doi: 10.1088/1402-4896/ad7d42.
45 Wu C, Li Y, Li Q, Ma Z, Deng T, Li Z, *et al.*, *Acta Mater*, 2023, 260119324, doi: 10.1016/j.actamat.2023.119324.

46 Chandel M, Pratap Singh V, Jasrotia R, Singha K & Kumar R, *AIMS Mater Sci*, 73 (2020) 244, doi: 10.3934/matersci.2020.3.244.

47 Kimel A V & Zvezdin A K, *Photonics Insights*, 12 (2022) C03, doi: 10.3788/PI.2022.C03.

48 Lovesey S W, *Phys Rev B*, 10721 (2023) 214426, doi: 10.1103/PhysRevB.107.214426.

49 Mohammed M H, Horvat J, Cheng Z X & Cao S X, *Mater Sci Forum*, 2020, 98529, doi: 10.4028/www.scientific.net/MSF.985.29.

50 Vankudothu N, Srikanth B, Reddy S S K, Raju N, Reddy M S, Reddy C G, *et al.*, *Phys B Condens Matter*, 2024, 680415819, doi: 10.1016/j.physb.2024.415819.

51 Zhang F, Li S, Song J, Shi J, Sun X, *IEEE Trans Magn*, 5111 (2015)1, doi: 10.1109/TMAG.2015.2445916.

52 Wang Z Q, Mu Y, Zeng Z Y, Chen X R & Chen Q F, *Mater Res Express*, 65 (2019) 055605, doi: 10.1088/2053-1591/ab0694.

53 Yehia M, Ismail S M & Hashhash A, *J Supercond Nov Magn*, 273 (2014) 771, doi: 10.1007/s10948-013-2340-z.

54 Ahmad M N, Khan H, Islam L, Alnasir M H, Nisar Ahmad S, Qureshi M T, *et al.*, *J Mater Phys Sci*, 41 (2023) 32, doi: 10.52131/jmps.2023.0401.0034.

55 Soni H, Acevedo R, Obad S, Kumar B, Singh J, Bechelany M, Gupta M & De Matteis V, *E3S Web Conf*, 2024, 58802012, doi: 10.1051/e3sconf/202458802012.

56 Bockovs I, Zalite I, Kodols M, Heidemane G, Grabis J, Zicans J, *et al.*, *IOP Conf Ser Mater Sci Eng*, 2015, 77012046, doi: 10.1088/1757-899X/77/1/012046.

57 Tanbir K, Ghosh M P, Singh R K, Kar M & Mukherjee S, *J Mater Sci Mater Electron*, 311 (2020) 435, doi: 10.1007/s10854-019-02546-9.

58 Zhao X, Sun A, Zhang W, Yu L, Zuo Z, Suo N, *et al.*, *J Mater Sci Mater Electron*, 311 (2020) 762, doi: 10.1007/s10854-019-02583-4.

59 Maddileti J, Vidyasagar T & Krishna Reddy C V, *J Rare Earths*, 428 (2024) 1546, doi: 10.1016/j.jre.2023.08.011.

60 Sheikh F A, Khan Asghar H M N ul H, Khalid M, Gilani Z A, Ali S M, Khan N ul H, *et al.*, *Phys B Condens Matter*, 2023, 652414656, doi: 10.1016/j.physb.2023.414656.

61 Wang B J, Zhang X, Tang J, Li Y L, Lan M, Ren W N, *et al.*, *Mater Today Commun*, 2024, 39108924, doi: 10.1016/j.mtcomm.2024.108924.

62 Saha S, Acharya S, Srinivasan G, In 2024 IEEE SENSORS, 2024, 1, doi: 10.1109/SENSORS60989.2024.10784531.

63 Sekulic D L, Lazarevic Z Z & Romcevic N Z, In 2019 IEEE 31st International Conference on Microelectronics (MIEL), 2019, 95, doi: 10.1109/MIEL.2019.8889583.

64 Šimšová J, *Czechoslov J Phys*, 206 (1970) 727, doi: 10.1007/BF01690473.

65 Li X, Tan G, Chen W, Zhou B, Xue D, Peng Y, *et al.*, *J Nanoparticle Res*, 2012, 143, 751, doi: 10.1007/s11051-012-0751-6.

66 Atta S, Halder M, Meikap AK, *J Mater Sci Mater Electron*, 326 (2021) 6992, doi: 10.1007/s10854-021-05407-6.

67 Al-Senani G M, Al-Fawzan F F, Almufarij R S, Abd-Elkader O H & Deraz N M, *Crystals*, 1211 (2022) 1542, doi: 10.3390/cryst12111542.

68 Sedrati C, Alleg S, Boussafel H & Bendali Hacine A, *J Mater Sci Mater Electron*, 3219 (2021) 24548, doi: 10.1007/s10854-021-06932-0.

69 Raja, Alexander A, Sathyamoorthy B & Chandrasekaran G, 2019,020075, doi: 10.1063/1.5130285.

70 Kumar S, Rawat D, Singh R, Barman P B & Singh R R, *J Alloys Compd*, 2024, 976172867, doi: 10.1016/j.jallcom.2023.172867.

71 Mao R D, Zhang X, Li Y L, Lan M, Ren W N, Huang S J, *et al.*, *Ceram Int*, 502 (2024) 3139, doi: 10.1016/j.ceramint.2023.11.063.

72 Robbins K, Gorman M, Bowers J & Brockman R, *Chaos An Interdiscip J Nonlinear Sci*, 2004, 142, 467–76, doi: 10.1063/1.1688532.

73 Dinnebier R, *International Union of Crystallography Newsletter*, 2 (2001) 12.

74 Williamson G K & Hall W H, *Acta Metall*, 1953, 122.

75 Balzar D, Audebrand N, Daymond M R, Fitch A, Hewat A, Langford J I, *et al.*, *J Appl Crystallogr*, 376 (2004) 911, doi: 10.1107/S0021889804022551.

76 Subramanyam K N, *J Phys C Solid State Phys*, 415 (1971) 2266, doi: 10.1088/0022-3719/4/15/012.

77 O'bryan H M & Dimarcello F V, *J Am Ceram Soc*, 537 (1970) 413, doi: 10.1111/j.1151-2916.1970.tb12144.x.

78 Peng Y, Zhao X, Shao Y, Yue X, Hu Z & Huang S, *Adv Sci*, 2025, 125, doi: 10.1002/advs.202409024.

79 Shang M, Ren P, Wan Y & Lu X, *J Eur Ceram Soc*, 436 (2023) 2488, doi: 10.1016/j.jeurceramsoc.2023.01.033.

80 Ikram S, Jacob J, Mehboob K, Mahmood K, Amin N, Arshad M I, *et al.*, *J Supercond Nov Magn*, 347 (2021) 1833.

81 Randhawa B S, Singh J, Kaur H & Kaur M, *Ceram Int*, 366 (2010) 1993, doi: 10.1016/j.ceramint.2010.03.034.

82 Shetty P B, Maddani K I & Gumaste M R, *Phys Solid State*, 671 (2025) 27, doi: 10.1134/S1063783424601152.

83 Sinha A & Dutta A, *J Phys Chem Solids*, 2020, 145.

84 Guragain D, Rai B K, Yoon S, Poudel T P, Bhandari S C & Mishra S R, *Magnetochem* 61 (2020) 14, doi: 10.3390/magnetochemistry6010014.

85 Rajenimbalkar R S, Deshmukh V J, Patankar K K & Somvanshi S B, *Sci Rep*, 141 (2024) 29547, doi: 10.1038/s41598-024-81222-3.

86 Venugopal A D, Selvaraj S, Sahadevan J, Kim I, Ramalingam P & Paramasivam S, *Zeitschrift für Phys Chemie*, 23811 (2024) 2003, doi: 10.1515/zpch-2023-0485.

87 Mahu E, Samoila P, Ignat M, Cojocaru C & Harabagiu V, *Comptes Rendus Chim*, 25S3 (2022) 189, doi: 10.5802/crchim.157.

88 Gatchakayala N B & Dachuru R S R, *Phys status solidi*, 2023, 2607, doi: 10.1002/pssb.202300010.

89 Zhu Y J & Chen F F, *Encyclopedia of Nanomaterials Elsevier*, 2023, 48, doi: 10.1016/B978-0-12-822425-0.00067-1.

90 Yadav N, Jain P & Thakur O P, 2024, 193, doi: 10.1007/978-981-99-6766-7_17.

91 Sivaprakash P, Divya S, Esakki Muthu S, Ali A, Jaglicic Z, Hwan Oh T, *et al.*, *Mater Sci Eng B*, 2024, 301117200, doi: 10.1016/j.mseb.2024.117200.

92 Kumar S, Mondal C, Dutta A & Sinha A, *ECS J Solid State Sci Technol*, 137 (2024) 073017, doi: 10.1149/2162-8777/ad6503.

93 Panniello A, Binetti E, Ingrosso C, Curri M L, Agostiano A, Tommasi R, *et al.*, *J Nanoparticle Res*, 154 (2013) 1567, doi: 10.1007/s11051-013-1567-8.

94 Mayakkannan M, Thangarasu S, Siva V, Murugan A, Shameem A & Asath Bahadur S, *Mater Sci Eng B*, 2024, 306117448, doi: 10.1016/j.mseb.2024.117448.

95 Bhuvaneshwari V, Lenin N, Shiva C, Kathirvel M, Ragavendran V, Rajeshwari A, *et al.*, *Mater Sci Eng B*, 2023, 288116184, doi: 10.1016/j.mseb.2022.116184.

96 Kumar A, Sharma P, Fujun Q, Jiang H & Jin C, *Adv Mater*, 131 (2024) 16, doi: 10.11648/j.am.20241301.13.

97 Shubhra, Singh R K, Kumar N, Kumar V, Das S B & Siddiqui M M H, *Appl Phys A*, 12711, (2021) 861, doi: 10.1007/s00339-021-05011-9.

98 Ateia E, Ahmed M A & Ghouniem R M, *Int J Mod Phys B*, 2919 (2015) 1550126, doi: 10.1142/S021797921550126X.

99 Rao P V S, Anjaneyulu T, Reddy D V K & Reddy M R, *Adv Mater Phys Chem*, 0810 (2018) 401, doi: 10.4236/ampc.2018.810027.

100 Farid M T, Ahmad I, Aman S, Kanwal M, Murtaza G, Ali I, *et al.*, *Dig J Nanomater Biostructures*, 101 (2015) 265.

101 Dwevedi S, Bharathi K K & Markandeyulu G, *IEEE Trans Magn*, 4510 (2009) 4253, doi: 10.1109/TMAG.2009.2023869.

102 Almessiere M A, Unal B, Slimani Y, Gungunes H, Toprak M S, Tashkandi N, *et al.*, *J Mater Res Technol*, 2021, 142534, doi: 10.1016/j.jmrt.2021.07.142.

103 Sinha A, Dutta A, *Phys status solidi*, 2018, 21511, doi: 10.1002/pssa.201700908.

104 Kareem S J, Al-Aaraji M N & Hatem A, *Solid State Phenom*, 2023, 34157.

105 Sowjanya P, Pavan Kumar N, Chelvane A & Ramana Reddy M V, *Mater Sci Eng B*, 2023, 297116753, doi: 10.1016/j.mseb.2023.116753.

106 Phugate D V, Borade R B, Kadam S B, Dhale L A, Kadam R H, Shirsath S E, *et al.*, *J Supercond Nov Magn*, 3311 (2020) 3545, doi: 10.1007/s10948-020-05616-w.

107 Nag S, Das D & Mukherjee S, 2019, 040003, doi: 10.1063/1.5122340.

108 Srinivasamurthy K M, Angadi V J, Kumar P M, Nagaraj B S, Deepthy P R, Pasha U M, *et al.*, 2018, 030277, doi: 10.1063/1.5032612.

109 Mahalakshmi S, Srinivasa M K & Nithiyanantham S, *J Mater Sci Mater Electron*, 283 (2017) 3060, doi: 10.1007/s10854-016-5893-3.

110 Atta S, Halder M & Meikap A K, 2020, 030436, doi: 10.1063/5.0017006.

111 Ditta A, Khan M A, Junaid M, Khalil R M A & Warsi M F, *Phys B Condens Matter*, 2017, 50727–34, doi: 10.1016/j.physb.2016.11.030.

112 Bharathi K K, Markandeyulu G, Ramana C V, *Electrochem Solid-State Lett*, 1311 (2010) G98, doi: 10.1149/1.3479553.

113 Ranga R, Kumar K, Kumar A, *Ceram Int*, 4920 (2023) 33333.

114 Luo GS, Zhou W P, Li J D, Zhou Z Y, Jiang GW, Li WS, *et al.*, *J Mater Sci Mater Electron*, 2810 (2017) 7259, doi: 10.1007/s10854-017-6408-6.

115 Awati V, Badave K & Bobade D, *Indian J Phys*, 961 (2022) 89, doi: 10.1007/s12648-020-01955-5.

116 Paswan S K, Kumar P, Kumari S, Datta S, Kar M, Borah J P, *et al.*, *J Alloys Compd*, 2024, 973172830, doi: 10.1016/j.jallcom.2023.172830.

117 Akhtar P, Akhtar M N, Baqir M A, Ahmad A, Khallidoon M U, Farhan M, *et al.*, *J Mater Sci Mater Electron*, 326 (2021) 7692, doi: 10.1007/s10854-021-05487-4.

118 Nagesh G V, Dhanalakshmi B & Ramesh K V, *Integr Ferroelectr*, 2301 (2022) 138–47, doi: 10.1080/10584587.2022.2102806.

119 Anu K S & Vishnumurthy K A & Natarajan K, *J Mines, Met Fuels*, 2024, 134, doi: 10.18311/jmmf/2024/47252.

120 Sulaiman J M A, Calinescu I, *Adv Mater Process Technol*, 82 (2022) 1312, doi: 10.1080/2374068X.2020.1856635.

121 Kotwal P, Jasrotia R, Himanshi, Prakash J, Kandwal A, Raja V, *et al.*, Singh J, Bhattu M, editors. *E3S Web Conf*, 2024, 50901011, doi: 10.1051/e3sconf/202450901011.

122 Alzahrani F M A, Irshad A, Zulfiqar S, Alrowaili Z A, Ain N ul, Anwar A, *et al.*, *J Rare Earths*, 4112 (2023) 1919, doi: 10.1016/j.jre.2023.07.020.

123 Alburaih H A, ul Haq M A, Jabbar A, ur Rehman A, Laref A, Saad Hasb Elkhalig M M, *et al.*, *Magnetochemistry*, 107 (2024) 48, doi: 10.3390/magnetochemistry10070048.